

X-Ray Analysis of a Lockman Hole Quasar at Redshift 1.958

Niklas Engelhardt Örne
niklas.onne@au.se

under the direction of
Dennis Alp
Department of Physics
KTH Royal Institute of Technology

Naturvetenskaplig specialisering
inr. Astronomi
HT2019 - VT2020

Blackebergs gymnasium
May 18, 2020

Abstract

Active galactic nuclei (AGNs) are the compact central region of galaxies and mainly differ from normal galactic nuclei in their luminosity. The extreme power is thought to originate from the accretion of matter onto a central supermassive black hole (SMBH) in a highly efficient process. Quasars, a type of AGN, can be some of the most luminous objects in the Universe, outshining entire galaxies, and are consequently interesting to study. As the AGN interacts with its surroundings, different physical phenomena correspond to signature emission features. Studying the spectra of AGNs is thus effective in understanding the physics of black holes and accretion disks. In this study an X-ray spectral analysis of the redshift 1.958 Lockman hole quasar J105331.8+572454 is presented using data from the *XMM-Newton* observatory. A power law with an additional Gaussian component was fitted to the data using the software *XSPEC*. The intrinsic luminosity in units of 10^{44} erg s $^{-1}$ was calculated to $L_{44} = 11.13 \pm 0.36$ in the 2 – 10 keV band, and was then used to find an estimate for the black hole mass. Using bolometric correction factors and accretion rates from the literature, it was calculated to $M_{\text{BH}} = 5 \times 10^9 M_{\odot}$. The goodness of the fit and relation between photon index and luminosity can be seen as possible evidence for the existence of a relativistic jet originating from the nucleus. The observed source has not yet been detected in the radio band, and as jets are characterized by strong radio emission, further studies on the target would be interesting.

Acknowledgements

I would like to express my gratitude to my mentor in this project, Dennis Alp, for teaching me the concepts and for making this possible. His help and support has been essential. Additionally, I am thankful to Kerstin Francke for her encouragement.

Contents

1	Introduction	1
1.1	Aim	1
2	Background	1
2.1	Electromagnetic Spectrum	1
2.1.1	Spectroscopy	2
2.1.2	Doppler Shift	2
2.2	Spectra of AGN	2
2.2.1	Classification	3
2.2.2	X-ray Spectrum	3
2.3	Eddington Limit	4
2.4	<i>XMM-Newton</i>	4
3	Methods	5
3.1	Selection of Target	5
3.2	Fitting Models	6
3.3	Model Components	6
3.4	Calculations	6
3.4.1	Black Hole Mass	6
3.4.2	Size of Emitting Region	8
4	Results	8
5	Discussion	8
5.1	Spectrum Components	8
5.1.1	Evidence for Jets	9
5.1.2	Weak and Narrow Line Emission	9
5.2	Errors in Calculating Black Hole Mass	9
5.3	Eddington Ratio	9
5.4	Time Scale of Variability	9
5.5	Further Research	10
6	Conclusion	10
	References	11
A	Light Curves	14

1 Introduction

An active galactic nucleus, AGN, is the compact central part of a galaxy and mainly differs from normal galactic nuclei in its luminosity. Generally, AGNs have intrinsic luminosities of $L \sim 10^{45}$ erg s^{-1} ($2.5 \times 10^{11} L_{\odot}$, where L_{\odot} is the luminosity of the sun), though their luminosities vary over nine orders of magnitude and they can be some of the most luminous persistent sources of radiation in the Universe. It has for a long time been argued that AGNs are powered by the accretion of matter onto supermassive black holes, or SMBHs, with masses of $10^6 - 10^{10} M_{\odot}$ (Lynden-Bell 1969; Kazanas et al. 2012). More recent observations have suggested the presence of a SMBH in the centers of most, if not all, major galaxies (Kormendy and Richstone 1995; Magorrian et al. 1998), which suggests that normal galactic nuclei are dead AGNs.

In galaxies where the SMBH is in a dense environment, it may accrete significant amounts of matter from its surroundings. The angular momentum of the infalling material causes it to form a rotating, flattened disk known as an accretion disk. As the matter falls in toward the black hole, the gravitational potential energy of the material gets converted into radiation in the highly efficient¹ accretion process. This results in the extreme luminosity of some AGNs.

In the early 20th century, the physical nature of AGNs was not entirely understood, though some properties of these objects had been observed; e.g. the discovery of a particle jet seemingly originating from the center of Messier 87 (Fath 1909; Curtis 1918). According to current estimates, roughly 10% of AGN have such relativistic jets which can extend for several million light years (Mezcua and Prieto 2014). This implies that they have pointed in the same direction for a long time, which suggests that the central object producing them is stable. In other words, the emitting region seems to have gyroscopic properties like those of a rotating body. This is explained by the angular momentum of the accretion disk.

The nature of the energy output, the apparent luminosity and the size of AGNs differ significantly between galaxies as they are dependent on many parameters. Generally, AGNs are classified accordingly as will be explained in section 2.2.1.

¹Black hole accretion can have an efficiency of $\sim 30\%$, compared to e.g. H to He fusion which only has an efficiency of $\sim 0.7\%$.

1.1 Aim

This study aims to investigate a previously unstudied Lockman hole quasar at $z = 1.958$ through an X-ray analysis. The Lockman hole is a well-known and extensively observed field. Therefore, a detailed analysis of this relatively strong X-ray source is very interesting.

2 Background

Observed variability in AGN luminosity over short time scales of days or less restricts the size of the source of radiation to a comparably small region of space due to causality. In other words, the speed of variability is confined by the time it takes light to travel across the emitting region. Even though it can outshine entire galaxies, the emitting area of an active galactic nucleus is so tiny in comparison to its host galaxy, that, in most cases, it is impossible to resolve any details through observation. Consequently, it becomes necessary to meticulously analyze the characteristics of the emitted radiation. Over the past few decades, many methods have been developed to break electromagnetic radiation into its core components. The purpose of this section is to describe some useful methods to analyze the light coming from distant extragalactic sources as well as provide an explanation for how the different components of the spectra correspond to different physical phenomena.

2.1 Electromagnetic Spectrum

All photons carry with them a certain amount of energy. The energy of a photon is $E = hc/\lambda$, where h is the Planck constant, c is the speed of light and λ is the wavelength of the photon. Thus, the shorter the wavelength, the greater the energy and vice versa. A spectrum is essentially the energy distribution of the electromagnetic radiation, i.e. light, emitted or reflected by an object.

The colored part of the electromagnetic spectrum in figure 1 represents the wavelengths of light visible to humans. To see other wavelengths, instruments and detectors are needed. In astronomy, this becomes essential as celestial objects emit radiation over large portions of the spectrum. The target of this study is a strong source of X-rays. Photons are said to be X-rays if their wavelength is in the range $0.01 - 10$ nm, which corresponds to energies of 100 eV $- 100$ keV. Note that 1 eV $\approx 1.602177 \times 10^{-19}$ J. High-energy X-ray photons are referred to as “hard” and low-energy photons as “soft”.

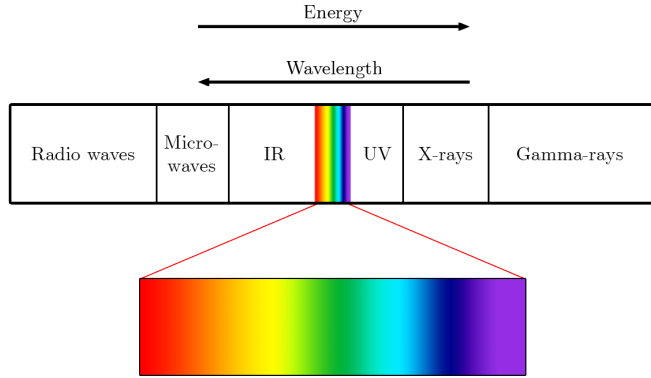


Figure 1: The electromagnetic spectrum.

2.1.1 Spectroscopy

A powerful tool to analyze radiation is spectroscopy. It is a way of dividing light into its constituent wavelengths. Thus, it allows precise analysis of the nature of the light, which is fundamental for astronomy. Modern camera X-ray sensors in telescopes detect individual photons and measure their energy, ultimately generating a list of positions and energies of detected photons. This list can then be used to create a spectrum. One way spectra can carry information is through emission and absorption lines. Emission lines are spikes, or lines, in the spectrum indicating the presence of certain elements as all elements emit light of particular quantized wavelengths. Absorption lines are dark lines, or troughs, in the spectrum representing the absence of specific wavelengths, suggesting the presence of absorbing elements between the light source and the observer. Thus, spectroscopy can be used to determine the components of astronomical objects.

2.1.2 Doppler Shift

When an observer is moving relative to a source of waves, the frequency or wavelength of the waves seem to change. This change is called the Doppler shift. For light, this is seen as a shift of the electromagnetic spectrum, usually called redshift or blueshift depending on the direction of motion.

Astronomically, Doppler shift is an important effect. In 1929, the astronomer Edwin Hubble published a paper relating the redshift, and therefore the recessional velocity, of astronomical objects to their distance from the Earth (Hubble 1929). This has since become known as Hubble-Lemaitre's law and is an effect of the expansion of space. As the space between galaxies is stretched, distant objects

appear to be moving away from us², resulting in a redshift. The law is expressed as

$$v = H_0 D, \quad (2.1)$$

where v is the recessional velocity of the source, D its distance from Earth and H_0 the Hubble-Lemaitre constant. Note that this is a linear approximation that only holds for relatively nearby objects. This formula allows for calculation of the distance to a light source simply by measuring its spectral redshift:

$$1 + z = \sqrt{\frac{1 + v/c}{1 - v/c}} = \frac{\lambda_{\text{obs}}}{\lambda_0}, \quad (2.2)$$

where z is the observed redshift, v is the recessional velocity of the source, c is the speed of light and λ_{obs} and λ_0 are the observed and emitted wavelengths, respectively. It should be noted that the redshifts of continua are generally not measurable. To calculate the redshift, a reference feature, such as an emission line, is needed.

2.2 Spectra of AGN

The spectra of AGNs typically range over 10 orders of magnitude in energy, from low energies, i.e. radio, to higher energies like X-rays and in some cases even γ -rays. Different parts of the system contribute to different parts of the spectrum. The lower energy radiation, radio, is thought to mostly originate from bipolar jets extending from the black hole. Therefore, radio-quiet AGN are generally interpreted as non-jetted. In some cases, γ -rays can also be emitted by the jets. Optical and UV radiation is produced as thermal radiation from gas and

²This law is independent of position as every point in space appears as the center of expansion.

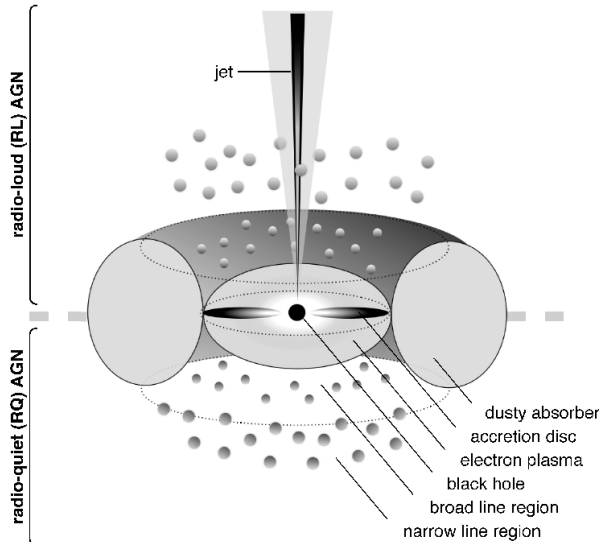


Figure 2: Illustration of the inner region of an active galactic nucleus. Image courtesy of Beckmann and Shrader (2012).

dust at an intermediate distance from the center. In the immediate vicinity of the black hole, X-rays are emitted.

The matter in the accretion disk moves at velocities of a significant fraction of the speed of light, and is consequently subject to relativistic effects. Like in the sun, magnetic flares occasionally erupt from this disk. As a consequence of different velocities at different radii of the infalling matter, the magnetic flares quickly rupture resulting in a coronal structure around the black hole. Due to different processes, high energy radiation such as X-rays is produced and emitted.

Moreover, some AGNs have relativistic particle jets extending from their innermost region (Marscher et al. 2002; Chatterjee et al. 2009; Chatterjee et al. 2011; Lohfink et al. 2013) (see figure 2), though the nature of their formation is still not entirely understood (Lohfink et al. 2017). The jets, which often come in pairs extending in opposite directions, are characterized by strong radio emission and contribute to the broad-band spectra of AGNs.

2.2.1 Classification

Active galactic nuclei are classified by observed properties. Generally, a distinction is made between radio-quiet and radio-loud AGN based on the ratio of their radio emission to their total bolometric³ luminosity. The first classification is known as *Seyfert*

³The bolometric luminosity is the total power output across all wavelengths.

galaxies after the astronomer Carl K. Seyfert who studied them in the 1940s (Seyfert 1943). Seyfert galaxies are in turn divided into two sub-groups; Seyfert 1s and 2s. Seyfert 1s have broad emission lines such as H α and H β (two types of hydrogen emission) as well as narrow lines, e.g. O III (a type of oxygen emission). Seyfert 2s have similar properties except for a lack of broad emission lines. Common for both types is that their narrow lines are broader than normal galaxies and that they have a relatively smooth continuum.

Another type of AGNs are *radio galaxies*, which are characterized by strong radio emission. The radio emission is thought to originate from relativistic particle jets extending from the central region containing the SMBH. Radio galaxies are, in the same manner as Seyfert galaxies, divided into those with broad emission lines and those with only narrow lines.

In the 1960s, a type of star-like objects with strong radio emission was discovered. Consequently, they were named quasi-stellar radio sources and were subsequently abbreviated *quasars*. After many years of discussion regarding the nature of quasars, it was suggested that they are a type of AGN, which is now widely accepted. Quasars can be some of the brightest objects in the known Universe, with typical bolometric luminosities of 5×10^{46} erg s⁻¹. Most quasars are observed at great distances, suggesting that their prevalence was more common in the early Universe (Carroll and Ostlie 2013). If the accretion disk of a quasar is almost perpendicular to the line of sight, their apparent luminosity is maximized. In such cases, they are referred to as *blazars*, and have spectral properties such as rapid variability, weak spectral lines and linearly polarized optical light (Gaidos et al. 1996; Sambruna et al. 1996; Krolik 1999).

2.2.2 X-ray Spectrum

The X-ray spectrum is thought to mostly originate from the coronal structures. Lower energy thermal photons from the accretion disk collide with electrons in the corona, which through an inverse Compton-scattering process boosts the energy of the photons into the X-ray range. This naturally gives rise to a power law spectrum, meaning that

$$N_E(E) \propto E^{-\Gamma}, \quad (2.3)$$

where N is the photon flux density of energy E and Γ represents the photon index. There is evidence for an inverse relationship between photon index and luminosity for AGN with jets (Abdo et al. 2010; Kataoka et al. 2008). Some of the X-rays

produced by the corona shine onto the accretion disk where they are either reflected via Compton-scattering or absorbed by the material in the disk. There is a competition between these two processes where the probability of the outcome is dependent on the energy of the photon. This results in a Compton reflection hump in the spectrum which can be modeled as a black body.

There is another possible outcome as well. Photons from the corona can interact with iron atoms in the accretion disk and excite the $n = 1$ electrons. As the other electrons in the atom falls down to fill the “hole”, a photon is emitted. This process is known as fluorescence and results in the Fe $K\alpha$ emission line. For neutral iron atoms, the $K\alpha$ -line is at 6.4 keV. The shape of this line is affected by different phenomena such as Newtonian Doppler shift, transverse Doppler shift, relativistic beaming and gravitational redshift. See e.g. Fabian et al. (2000) for a visualization of these effects.

Furthermore, as the corona has a finite temperature, it cannot produce photons of energies above a certain threshold. This results in a high energy cutoff which can be used to study the temperature of the corona.

At lower energies, a soft X-ray excess emission is normally seen. This phenomenon is not well understood, but the spectrum component can be roughly modeled as a blackbody. A possible explanation is that the soft excess is a combination of emission from the accretion disk and Compton scattering by the corona.

2.3 Eddington Limit

Astronomical structures, such as stars or AGNs, are sometimes found in a state of hydrostatic equilibrium, i.e. when the outward radiative force exactly balances the force of gravity acting inward. The maximum luminosity an object can have and still maintain hydrostatic equilibrium is known as the Eddington limit. The Eddington limit is thus when the photon pressure exactly balances the force of gravity in such a way that, were this limit to be exceeded, the object would eject the surrounding material. It is important to take this into account when modeling the extreme environments of accreting SMBHs such as those in AGNs.

Assuming spherical symmetry, dynamical equilibrium and that pure, ionized hydrogen is the only gas absorbing the radiation, a basic derivation can be made. The outward radiative force F_{rad} of an object of luminosity L as a function of distance r is

$$F_{\text{rad}} = \frac{L}{4\pi r^2 E} \times \frac{E}{c} \times \sigma_T, \quad (2.4)$$

where E is the photon energy, c the speed of light and $\sigma_T = 6.65 \times 10^{-29} \text{ m}^2$ is the Thomson cross section for electron scattering. In this formula, the first factor $L/(4\pi r^2 E)$ represents the number flux of photons, E/c is the momentum per photon and this is multiplied by the cross section σ_T , which corresponds to the interaction probability. The gravitational force (also as a function of the distance r) is

$$F_{\text{grav}} = \frac{GM}{r^2} (m_p + m_e), \quad (2.5)$$

where $G = 6.67 \times 10^{-11} \text{ m}^3 \text{ kg}^{-1} \text{ s}^{-2}$ is the gravitational constant, M is the mass of the object and m_p and m_e are the proton and electron mass, respectively. As the object is in a state of hydrostatic equilibrium, $F_{\text{rad}} = F_{\text{grav}}$. Thus, the Eddington luminosity L_{Edd} is obtained by

$$L_{\text{Edd}} = \frac{4\pi m_p G M c}{\sigma_T} \approx 1.3 \times 10^{38} \frac{M}{M_\odot} \text{ erg s}^{-1}, \quad (2.6)$$

where M_\odot is the mass of the sun. Here, the approximation has been made that $m_p + m_e \approx m_p$ as the electron is ~ 1800 times lighter than the proton (Melia 2009).

2.4 XMM-Newton

The data used in this study is from the *XMM Newton* telescope, which can detect X-rays in the range 0.1 – 15 keV. However, in practice, only the range 0.3 – 10 keV is used as it is better calibrated and generally has more photon detections. The telescope consists of three different telescopes mounted to the same spacecraft and has a field of view (FOV) of 30 arcmin (1 arcmin = $\frac{1}{60}$ of a degree). The main instrument, providing imaging and spectroscopy, is the European Photon Imaging Camera (EPIC). EPIC has three different cameras⁴ that are highly sensitive to X-rays and can be used for observations over the entire FOV of the telescope (Jansen et al. 2001). Because of effects such as vignetting and reflectivity, the geometric mirror area of a telescope does not represent the area that can be used to make sufficiently accurate observations. The latter is known as the effective area and depends on the energy of the photons. The effective area of *XMM-Newton* as a function of energy is shown in figure 3.

For any point-like source, the probability of detecting a photon follows a Gaussian distribution (also known as a normal distribution). The energy and angular resolution of any telescope is described

⁴The three cameras are called FM2-pn, FM3-MOS1 and FM4-MOS2, respectively.

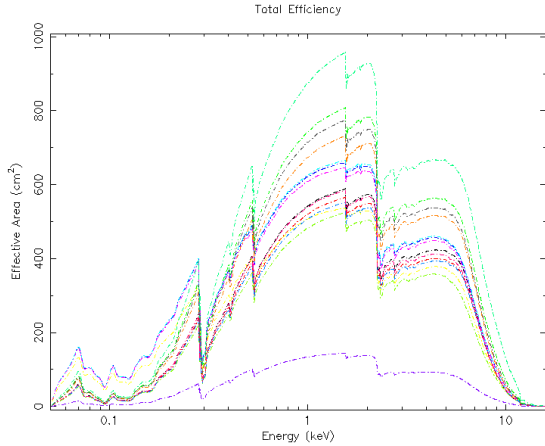


Figure 3: The effective area of the *XMM-Newton* observatory as a function of energy. This is different for each observation as it depends on where on the sensor the target is.

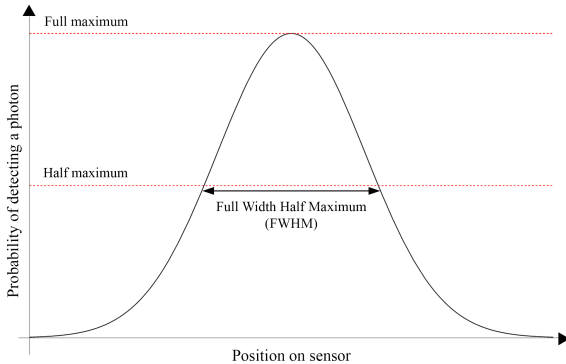


Figure 4: The Gaussian distribution of photon detection probability and definition of Full Width Half Maximum (FWHM).

by the FWHM (Full Width Half Maximum), which represents the area and energy where the probability of detecting a photon from a point-like source is exactly half that of detecting a photon where most photons are detected (see figure 4 for an illustration). This quantity depends on the energy of the photons. The energy and angular resolution of *XMM-Newton* is shown in table 1.

3 Methods

In this study, the X-ray data analysis software *XSPEC* (Arnaud 1996) was used for spectral analysis of the data. X-rays are subject to absorption by hydrogen and other elements in our Milky Way, the interstellar medium (ISM) and the host galaxy of the AGN. To obtain the intrinsic spectra of ex-

Sensor	FWHM (1.5 keV)	FWHM (8 keV)
FM2-pn	6.6	6.6
FM3-MOS1	6.0	5.1
FM4-MOS2	4.5	4.2

Table 1: Energy and angular resolution of *XMM-Newton* in units of arcseconds.

tragalactic sources, this needs to be taken into account. To calibrate the X-ray absorption, it is necessary to know the column density of hydrogen, N_H , along the line of sight to the source. In *XSPEC*, the model *tbabs* provides this normalization if given N_H (Wilms et al. 2000). The precise column density of hydrogen along the line of sight can be estimated from the X-ray data, but is better approximated by an online tool by Willingale et al. (2013) and fixed accordingly during spectral fitting. To compensate for the additional absorption of X-rays in the host galaxy, the model *ztbabs* (Wilms et al. 2000) can be used to calculate a parameter representing the resulting redshift.

3.1 Selection of Target

In every observation by *XMM-Newton*, a number of X-ray sources apart from the main target are detected in the field. This is a result of the wide FOV and high sensibility of the observatory. Thus, there are a lot of unstudied data of interesting X-ray sources in the archives. All data (except for those taken in the past 12 months) are publicly available.

The reviewed data in this study was a sample of variable X-ray sources from many different observations. Only the strongest sources in each observation were considered for selection. In general, the interesting targets were those classified as active galaxies in the data catalogues SIMBAD or NED with a count rate of at least 1 counts s^{-1} and which had previously not been thoroughly studied in the X-ray band. Observations with flares, that is with sudden spikes in the count rate, were preferred as the origin of the flares would be interesting to study.

The chosen target for the study is the quasar J105331.8+572454, which is located in the Lockman hole⁵ and has a redshift of $z = 1.958$. This specific target was chosen because it is a relatively strong source that has not previously been analyzed in detail despite the Lockman hole being an extensively studied and well-known field with a lot of data. Using $H_0 = 70 \text{ km s}^{-1} \text{ Mpc}^{-1}$, this red-

⁵Coordinates: Ra, Dec; (163.382°; 57.4151°).

shift corresponds to a comoving radial distance (obtained from equation 2.1) of ~ 16.9 Gly from Earth. The observation log is shown in table 2.

3.2 Fitting Models

The camera sensors do not directly obtain a spectrum, but rather a list of photons divided into different channels based on their energy. The photon count C as a function of the channel I is related to the actual spectrum of the source $f(E)$ by

$$C(I) = \int f(E)R(I, E)dE, \quad (3.1)$$

where $R(I, E)$ is the instrumental response. $R(I, E)$ is proportional to the probability that an incoming photon of energy E will be detected in channel I . To obtain the actual spectrum, this equation has to be inverted and solved for $f(E)$, which is very difficult to do. Consequently, it is best to approximate a model spectrum and adjust (“fit”) it to the data. Let $g(E, p_1, p_2, \dots)$ be a model spectrum with parameters (p_1, p_2, \dots) . Then, a predicted count spectrum $C_p(I)$ can be calculated and compared to $C(I)$. To judge how well the predicted count spectrum fits the observed one, a χ^2 goodness of fit test can be useful. It is calculated as

$$\chi^2 = \sum \frac{[C(I) - C_p(I)]^2}{(\sigma(I))^2}, \quad (3.2)$$

where $\sigma(I)$ is the error for channel I . This is generally unknown, but can be estimated by $\sigma(I) \approx \sqrt{C(I)}$ if there are sufficiently many detected photons in the channel⁶. The model parameters are then varied to find the best fit model $f_b(E)$ and parameters (p_{b1}, p_{b2}, \dots) .

3.3 Model Components

Many different models were tested, but the model that yielded the best fit was found to be

$$\text{MODEL 1} = \text{powerlaw} + \text{zgauss}$$

The component `powerlaw` describes a normal power law spectrum (equation 2.3) which is thought to originate from the coronal structures by Compton upscattering. The `zgauss` component represents a redshifted Gaussian curve which models the Fe $K\alpha$ -line.

In theory, the column density of hydrogen N_H along the line of sight should be taken into account

⁶This is generally said to be 25. If the number of photons are less, channels can be combined until there are enough photons in one bin.

as mentioned above, but it was found to be approximately zero for the coordinates of the studied source. Moreover, having the `tbabs` component in the model means having one more degree of freedom, which can influence the goodness of the fit. It was therefore left out. Likewise, the `ztbabs` component was found to be redundant as the host galaxy absorption was found to be negligible.

Other models that were tested included

$$\text{MODEL 2} = \text{tbabs}(\text{powerlaw})$$

$$\text{MODEL 3} = \text{tbabs}(\text{powerlaw} + \text{zgauss} + \text{kerrbb})$$

$$\text{MODEL 4} = \text{tbabs}(\text{powerlaw} + \text{relline} + \text{kerrbb} + \text{zgauss})$$

See (Li et al. 2005; Dauser et al. 2010; Dauser et al. 2013) descriptions of the model components. In all cases, the fit was generally not as good as for MODEL 1. Therefore, all calculations below are based on MODEL 1.

3.4 Calculations

3.4.1 Black Hole Mass

In order to calculate the mass of the central SMBH, the bolometric luminosity must be found as emission across all wavelengths affect the Eddington limit and the Eddington luminosity can be used to obtain the black hole mass (see equation 2.6). The bolometric luminosity L_{bol} is, for broadband sources like AGN, assumed to be proportional to the X-ray luminosity. The bolometric correction factor (proportionality constant) for luminosity in the 2 – 10 keV band follows the approximate relation (Netzer 2019)

$$\kappa = \frac{L_{\text{bol}}}{L_{2-10 \text{ keV}}} = 7 \times (L_{2-10 \text{ keV}}/10^{42} \text{ erg s}^{-1})^{0.3}. \quad (3.3)$$

The AGN is fueled by the conversion of mass to energy, which is described by the accretion efficiency η . The maximum energy emitted is thus $E = \eta M c^2$, where M is the mass available for conversion. As the bolometric luminosity is given by $L_{\text{bol}} = dE/dt$, the efficiency can be written as

$$\eta = L_{\text{bol}}/\dot{M}c^2, \quad (3.4)$$

where \dot{M} is the accretion rate. The rate can be calculated in units of the Eddington accretion rate, $\dot{m} = \frac{\dot{M}}{M_{\text{Edd}}}$, as

$$\dot{m} = \eta \frac{\dot{M}}{0.23M_8}, \quad (3.5)$$

Observation	Start time (UTC)	Stop time (UTC)	Exposure (ks)
2000			
1	April 27, 03:34:45	April 27, 20:48:15	62.0
2	April 29, 03:26:58	April 29, 20:38:41	61.9
3	May 2, 18:39:32	May 2, 23:14:51	16.5
4	May 19, 05:17:47	May 19, 15:45:18	37.7
2001			
5	October 25, 08:07:29	October 26, 06:35:30	80.9
6	October 27, 19:10:18	October 28, 12:18:59	61.7
7	November 4, 06:58:27	November 4, 17:12:43	36.9
2002			
8	October 19, 08:14:21	October 20, 09:08:29	89.6
9	October 21, 08:35:12	October 22, 07:22:39	82.0
10	October 23, 08:12:22	October 24, 12:22:21	101.4
11	October 25, 08:09:29	October 26, 13:02:42	104.0
12	October 27, 05:54:20	October 28, 05:10:00	83.7
13	November 27, 23:26:55	November 29, 09:55:26	124.1
14	December 4, 04:47:08	December 5, 08:17:54	99.0

Table 2: Observation log.

where \dot{M} is the accretion rate in units of solar masses per year and M_8 is the black hole mass in units of 10^8 solar masses (Bian and Zhao 2003). Thus, the mass of the black hole can be obtained by

$$M_8 = \frac{\kappa L}{0.23 \dot{m} c^2}, \quad (3.6)$$

where L is the luminosity of the AGN in the 2 – 10 keV band, κ the bolometric correction factor and c the speed of light.

3.4.2 Size of Emitting Region

As previously mentioned, the variability in brightness of the AGN is constrained by the time it takes light to travel across the emitting region. Accordingly, an upper bound on size of this region can be calculated by studying how the rate (photon counts per second) varies over time. However, such calculations are somewhat diffuse as will be discussed in section 5.4.

4 Results

The best fit of MODEL 1 resulted in a chi-squared value of 736.84. The photon indices of the power law are shown as a function of luminosity in figure 5. The average luminosity in the 2 – 10 keV band for all observations in units of 10^{44} erg s $^{-1}$ is $\bar{L}_{44} = 11.13 \pm 0.36$. This corresponds to a black hole mass of $M_{\text{BH}} = 5 \times 10^9 M_{\odot}$ (calculated from equation 3.6). No error is presented, the reason of which is discussed in section 5.2. In figure 6, the photon count rate is shown as a function of time for observation 12. All light curves for the observations in table 2 are shown in the appendix.

5 Discussion

The results show a spectrum made out of simple components, a high luminosity (and thus large BH mass), and relatively rapid variability of the studied source. Unfortunately, the uncertainties are large as the signal-to-noise ratio is low for sources this far away, although there are still interesting evidence for different physical phenomena being present in the AGN. In this section I will discuss possible explanations for and implications of the results.

5.1 Spectrum Components

As previously mentioned, different models with different components were fitted to the data, though only MODEL 1 resulted in a good fit. MODEL 3 and MODEL 4, which both have the dimensionless black

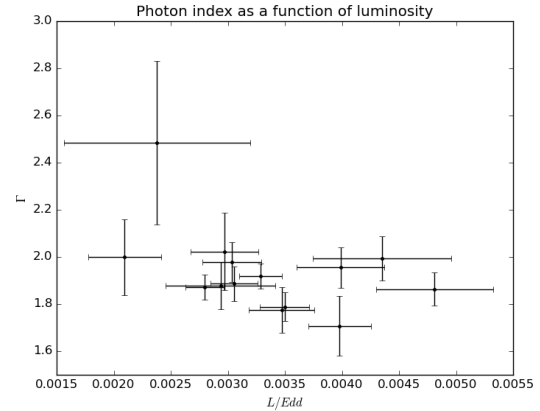


Figure 5: Photon index as a function of luminosity for MODEL 1.

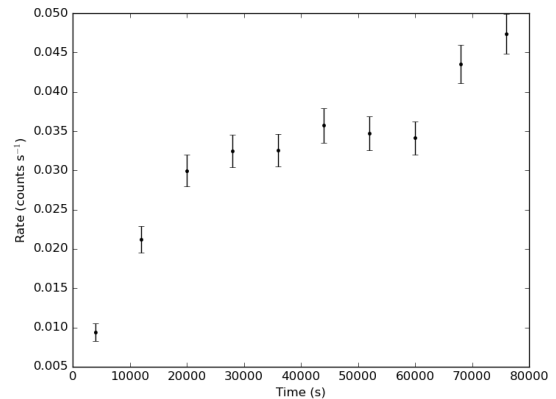


Figure 6: Photon count rate as a function of time for observation 12, see table 2.

hole spin⁷ parameter a as a free parameter, were difficult to fit to the data. Specifically, the spin parameter was difficult to constrain. There could be many reasons for this. One is that the data is simply too poor to constrain the spin parameter sufficiently, but it could also be that there are obstructions in the AGN along the line of sight. However, the latter would imply absorption in the host galaxy and no significant absorption was seen in the data. Furthermore, the large distance to the source and its low apparent magnitude decreases the signal-to-noise ratio.

Additionally, in order to constrain the spin parameter, strong reflection features are usually needed. The lack of such features is likely to have contributed to the large uncertainties.

⁷This represents the angular momentum of the black hole.

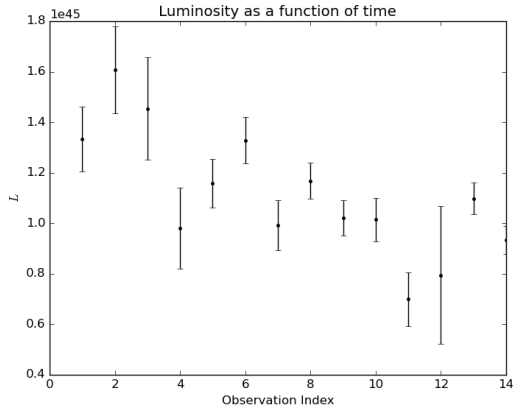


Figure 7: Luminosity as a function of time (observation index, see table 2). Note that the horizontal axis is not linear as the observations are not evenly distributed in time.

5.1.1 Evidence for Jets

Previous studies have found that jetted AGN normally give pure power law spectra (Urry and Shafer 1983) so the fact that a plain power law component gave such a good fit could be an indication of a jet. Moreover, the Gaussian component of MODEL 1 seems to indicate the presence of a weak Fe $K\alpha$ -line. This, together with the lack of soft excess, can also be an indication that the AGN is dominated by a jet as the reflection components are outshone by the jet (Kataoka et al. 2008).

Although there is no clear correlation between photon index and luminosity (see figure 5), the results are not inconsistent with the theory that jetted high luminosity AGNs are “harder when brighter” (Yang et al. 2015; Abdo et al. 2010; Kataoka et al. 2008).

5.1.2 Weak and Narrow Line Emission

The observed Fe $K\alpha$ emission line is very weak and narrow, which corresponds to the high luminosity of the AGN through the “X-ray Baldwin effect” (Iwasawa and Taniguchi 1993). As this is a reflection component, one explanation is that the emission-line region is far away from the black hole (Fabian et al. 2000; Iwasawa and Taniguchi 1993). This model also predicts high ionization, the nature of which depends on the thermal stability of the disk (Nayakshin et al. 2000). The temperature of the disk, and thus some of its thermal properties, could possibly be studied by finding the high-energy cutoff.

5.2 Errors in Calculating Black Hole Mass

As the luminosity scales linearly with the black hole mass according to equation 3.6, the error in the estimation of M_{BH} should be proportional to the statistical error in the luminosity. However, there is an additional uncertainty related to the value of \dot{m} as I used the approximate mean accretion rate from Bian and Zhao (2003). This then results in systematic errors from the model which are difficult to quantify. I have excluded errors from the obtained results for this reason. The computed values should consequently be regarded as an indication or reference rather than actual values.

Furthermore, the bolometric correction κ contributes to the uncertainty as well. The unknown radiation pattern of the X-ray corona is a possible source of uncertainty in the calculations of κ (Netzer 2019).

5.3 Eddington Ratio

The black hole mass can be used to determine the Eddington luminosity from equation 2.6. The Eddington ratio, defined as $L_{\text{bol}}/L_{\text{Edd}}$, is thus about 10 per cent for the observed source. It is believed that the Eddington ratio has an influence on the physical properties of the accretion disk (Boroson and R. F. Green 1992; Shen and Ho 2014; Churazov et al. 2005). Previous studies have found that the Eddington ratio and accretion rate can be used to separate radio-quiet from radio-loud quasars. Following the models of Boroson (2002), we would expect J105331.8+572454 to be radio-loud. This corresponds to the jet predictions as well.

There are suggestions that the lack of a strong Fe $K\alpha$ emission line may imply that the SMBH is accreting close to the Eddington limit (Nandra et al. 1995) as the inner parts of the disk expand from radiation pressure. This is a less plausible explanation for the observed weakness of the Fe $K\alpha$ -line because of the low Eddington ratio, but further studies could explore this in more detail.

5.4 Time Scale of Variability

As can be seen in figure 6, the rate varies by a factor ~ 2 over a time scale of about one day. Accounting for relativistic effects, this corresponds to a emission region size of $1/(1+z) \approx 0.34$ light days, or approximately $0.6 r_s$, where r_s is the Schwarzschild radius (radius of the black hole). This is in well accordance with the standard models of AGNs. It might be worth noting that we see similar variation on small and large time scales, see figures 6 and 7.

The concept of estimating emission region size from the time scale of variability in this manner is somewhat diffuse. First, the argument is based on the vague idea that if the emission region size were to be larger than $\sim 0.6 r_s$ across, it would not be able to vary as quickly as it does. Of course, the flux variation time must not equal the light crossing time, but it is a fairly reasonable assumption. Second, there is no clear definition of how the intrinsic variability is extrapolated from the data as many factors affect the rate; e.g. non-static obstructions along the line of sight, noise and solar wind. These factors as well as errors and uncertainty make it difficult to constrain the time of variability. Generally, actual variations in the rate or luminosity can be distinguished from the observational background as the former is relatively smooth compared to the latter. Thus, we can conclude that the variability seen in figure 6 is likely a consequence of intrinsic dynamics of the nucleus, which restricts the emission region size to the time scale of the observation. This observation can be compared to the spike in observation 5 (see figure 12 in appendix), which is more likely to be a consequence of solar activity.

5.5 Further Research

It would definitely be interesting to observe J105331.8+572454 in the radio band as it could confirm the presence of a jet. Follow up radio observations will possibly (not unlikely) find strong radio emission from the source, the character of which could be used to determine the orientation

of the quasar. Moreover, a more thorough analysis of the implications of the observed Eddington ratio would be valuable as it is closely related to the evolution of the SMBH (Merloni and Heinz 2008; Kauffmann and Heckman 2009). Determining the temperature of the disk would also be valuable as it could be combined with the line profile to explain the geometry of the region close to the black hole.

6 Conclusion

An X-ray analysis of the luminous Lockman hole quasar J105331.8+572454 has been presented. The best fit model was a simple power law with an additional Gaussian component corresponding to a weak iron $K\alpha$ -emission line. The clean power law model, weak emission line, possible anti-correlation between photon index and luminosity, and Eddington ratio is evidence that the emission is dominated by a relativistic jet, in which case we would expect a certain amount of radio emission. As the target has yet to be detected in the radio band, follow up radio observations would be interesting. The narrow Fe $K\alpha$ -line profile and lack of soft excess suggests that the reflecting region is relatively far from the black hole and could be an indication of a higher Eddington ratio than calculated. Moreover, the black hole mass is estimated, but with great uncertainties due to statistical and systematic errors. Rapid variability on small time scales indicates a small emission region on the order of light hours, which is in accordance with the standard models of AGNs.

References

- Abdo, AA et al. (2010). “Spectral properties of bright Fermi-detected blazars in the gamma-ray band”. In: *The Astrophysical Journal* 710.2, p. 1271.
- Arnaud, KA (1996). “Astronomical data analysis software and systems V”. In: *ASP Conf.* Vol. 17.
- Beckmann, Volker and Chris Shrader (2012). “Zu Inhaltsverzeichnis schnell und portofrei erhältlich bei”. In:
- Bian, Wei-Hao and Yong-Heng Zhao (2003). “Accretion rates and the accretion efficiency in AGNs”. In: *Publications of the Astronomical Society of Japan* 55.3, pp. 599–603.
- Boroson, Todd A (2002). “Black hole mass and eddington ratio as drivers for the observable properties of radio-loud and radio-quiet QSOs”. In: *The Astrophysical Journal* 565.1, p. 78.
- Boroson, Todd A and Richard F Green (1992). “The emission-line properties of low-redshift quasi-stellar objects”. In: *The Astrophysical Journal Supplement Series* 80, pp. 109–135.
- Carroll, Bradley W and Dale A Ostlie (2013). *Introduction to Modern Astrophysics, An: Pearson New International Edition*. Pearson Higher Ed.
- Chatterjee, Ritaban et al. (2009). “DISK–JET CONNECTION IN THE RADIO GALAXY 3C 120”. In: *The Astrophysical Journal* 704.2, p. 1689.
- Chatterjee, Ritaban et al. (2011). “Connection between the accretion disk and jet in the radio galaxy 3C 111”. In: *The Astrophysical Journal* 734.1, p. 43.
- Churazov, Eugene et al. (2005). “Supermassive black holes in elliptical galaxies: switching from very bright to very dim”. In: *Monthly Notices of the Royal Astronomical Society: Letters* 363.1, pp. L91–L95.
- Curtis, Heber Doust (1918). “Descriptions of 762 nebulae and clusters photographed with the Crossley reflector”. In: *Publications of Lick Observatory* 13, pp. 9–42.
- Dauser, Thomas et al. (2013). “Irradiation of an accretion disc by a jet: general properties and implications for spin measurements of black holes”. In: *Monthly Notices of the Royal Astronomical Society* 430.3, pp. 1694–1708.
- Dauser, T et al. (2010). “Broad emission lines for a negatively spinning black hole”. In: *Monthly Notices of the Royal Astronomical Society* 409.4, pp. 1534–1540.
- Fabian et al. (2000). “Broad iron lines in active galactic nuclei”. In: *Publications of the Astronomical Society of the Pacific* 112.775, p. 1145.
- Fath, Edward Arthur (1909). “The spectra of some spiral nebulae and globular star clusters”. In: *Publications of the Astronomical Society of the Pacific* 21.126, pp. 138–143.

- Gaidos, James A et al. (1996). “Extremely rapid bursts of TeV photons from the active galaxy Markarian 421”. In: *Nature* 383.6598, pp. 319–320.
- Hubble, Edwin (1929). “A relation between distance and radial velocity among extra-galactic nebulae”. In: *Proceedings of the national academy of sciences* 15.3, pp. 168–173.
- Iwasawa, Kazushi and Yoshiaki Taniguchi (1993). “The X-ray Baldwin effect”. In: *The Astrophysical Journal* 413, pp. L15–L18.
- Jansen, F et al. (2001). “XMM-Newton observatory-I. The spacecraft and operations”. In: *Astronomy & Astrophysics* 365.1, pp. L1–L6.
- Kataoka, J et al. (2008). “Multiwavelength Observations of the powerful gamma-ray quasar PKS 1510–089: Clues on the jet composition”. In: *The Astrophysical Journal* 672.2, p. 787.
- Kauffmann, Guinevere and Timothy M Heckman (2009). “Feast and Famine: regulation of black hole growth in low-redshift galaxies”. In: *Monthly Notices of the Royal Astronomical Society* 397.1, pp. 135–147.
- Kazanas, Demosthenes et al. (2012). “Toward a unified AGN structure”. In: *arXiv preprint arXiv:1206.5022*.
- Kormendy, John and Douglas Richstone (1995). “Inward bound—the search for supermassive black holes in galactic nuclei”. In: *Annual review of astronomy and Astrophysics* 33.1, pp. 581–624.
- Krolik, Julian Henry (1999). *Active galactic nuclei: from the central black hole to the galactic environment*. Princeton University Press.
- Li, Li-Xin et al. (2005). “Multitemperature blackbody spectrum of a thin accretion disk around a Kerr black hole: model computations and comparison with observations”. In: *The Astrophysical Journal Supplement Series* 157.2, p. 335.
- Lohfink, Anne M et al. (2013). “An X-ray view of the jet cycle in the radio-loud AGN 3C120”. In: *The Astrophysical Journal* 772.2, p. 83.
- Lohfink, Anne M et al. (2017). “The X-ray reflection spectrum of the radio-loud quasar 4C 74.26”. In: *The Astrophysical Journal* 841.2, p. 80.
- Lynden-Bell, Donald (1969). “Galactic nuclei as collapsed old quasars”. In: *Nature* 223.5207, pp. 690–694.
- Magorrian, John et al. (1998). “The demography of massive dark objects in galaxy centers”. In: *The Astronomical Journal* 115.6, p. 2285.
- Marscher, Alan P et al. (2002). “Observational evidence for the accretion-disk origin for a radio jet in an active galaxy”. In: *Nature* 417.6889, p. 625.
- Melia, Fulvio (2009). “High-energy astrophysics”. In:

- Merloni, Andrea and Sebastian Heinz (2008). “A synthesis model for AGN evolution: supermassive black holes growth and feedback modes”. In: *Monthly Notices of the Royal Astronomical Society* 388.3, pp. 1011–1030.
- Mezcua, M and MA Prieto (2014). “Evidence of parsec-scale jets in low-luminosity active galactic nuclei”. In: *The Astrophysical Journal* 787.1, p. 62.
- Nandra, K et al. (1995). “X-ray spectra of two quasars at $z > 1$ ”. In: *Monthly Notices of the Royal Astronomical Society* 276.1, pp. 1–8.
- Nayakshin, Sergei, Demosthenes Kazanas, and Timothy R Kallman (2000). “Thermal instability and photoionized X-ray reflection in accretion disks”. In: *The Astrophysical Journal* 537.2, p. 833.
- Netzer, Hagai (2019). “Bolometric correction factors for active galactic nuclei”. In: *Monthly Notices of the Royal Astronomical Society* 488.4, pp. 5185–5191.
- Sambruna, Rita M, Laura Maraschi, and C Megan Urry (1996). “On the spectral energy distributions of blazars”. In: *The Astrophysical Journal* 463, p. 444.
- Seyfert, Carl K (1943). “Nuclear Emission in Spiral Nebulae.” In: *The Astrophysical Journal* 97, p. 28.
- Shen, Yue and Luis C Ho (2014). “The diversity of quasars unified by accretion and orientation”. In: *Nature* 513.7517, pp. 210–213.
- Urry, Claudia Megan and Richard Arrick Shafer (1983). “Luminosity enhancement in relativistic jets and altered luminosity functions for beamed objects”. In:
- Willingale, Richard et al. (2013). “Calibration of X-ray absorption in our Galaxy”. In: *Monthly Notices of the Royal Astronomical Society* 431.1, pp. 394–404.
- Wilms, J, A Allen, and R McCray (2000). “On the absorption of X-rays in the interstellar medium”. In: *The Astrophysical Journal* 542.2, p. 914.
- Yang, Qi-Xiang et al. (2015). “Correlation between the photon index and X-ray luminosity of black hole X-ray binaries and active galactic nuclei: observations and interpretation”. In: *Monthly Notices of the Royal Astronomical Society* 447.2, pp. 1692–1704.

A Light Curves

Below are the light curves (rate vs. time) of the observations in table 2.

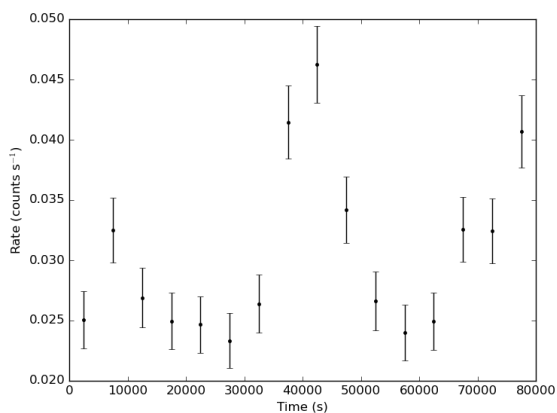


Figure 8: Observation 1, 5ks bins.

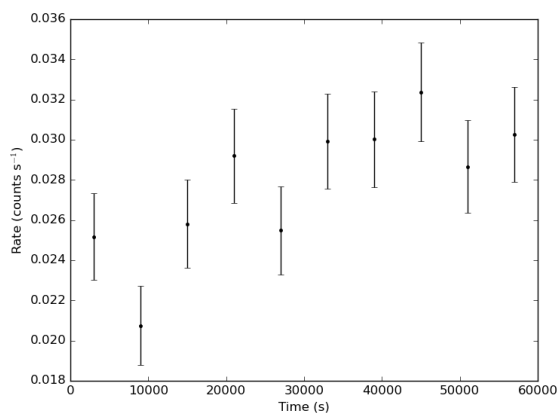


Figure 9: Observation 2, 6ks bins.

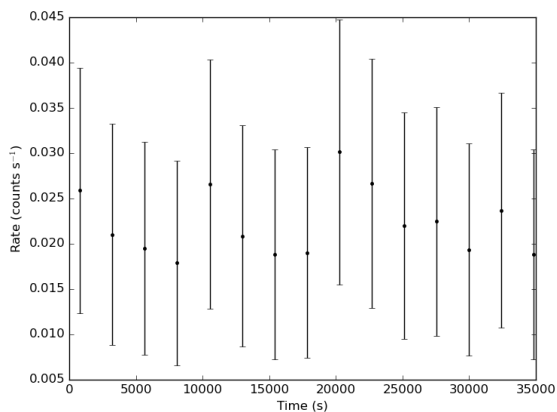


Figure 10: Observation 3, 3ks bins.

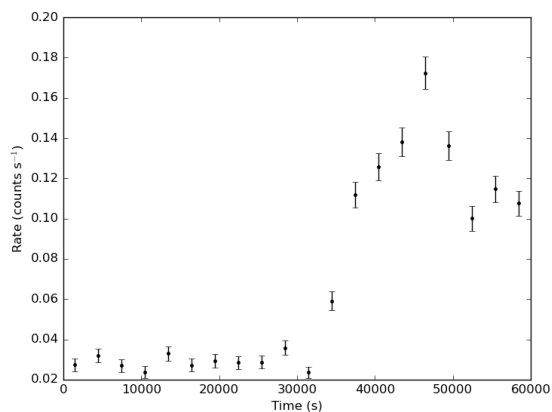


Figure 11: Observation 4, 3ks bins.

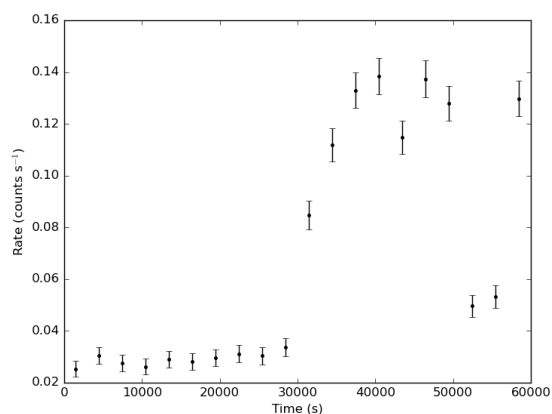


Figure 12: Observation 5, 3ks bins.

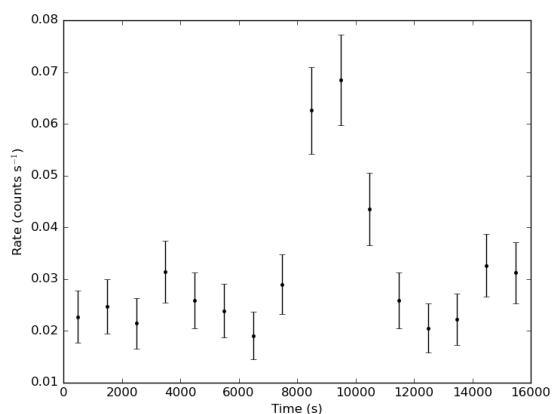


Figure 13: Observation 6, 1ks bins.

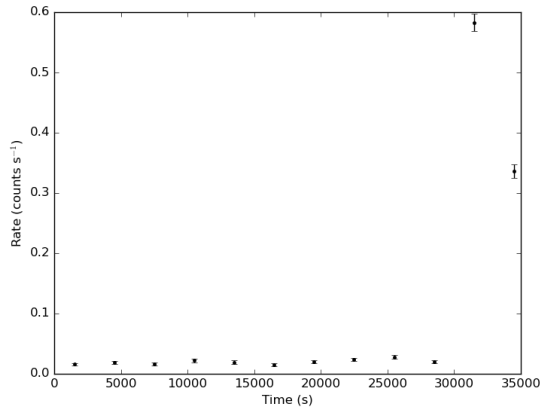


Figure 14: Observation 7, 3ks bins.

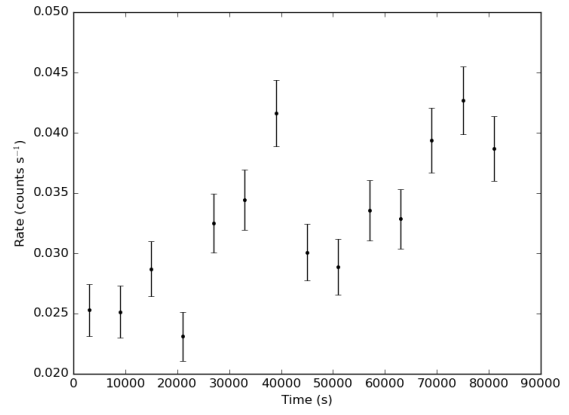


Figure 15: Observation 8, 6ks bins.

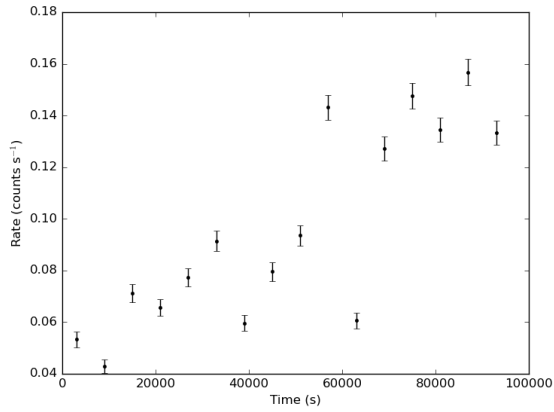


Figure 16: Observation 9, 6ks bins.

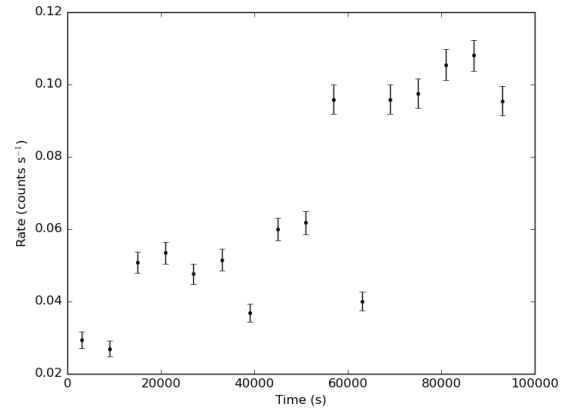


Figure 17: Observation 10, 6ks bins.

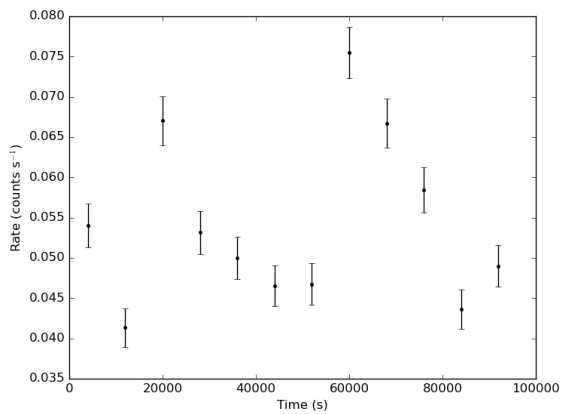


Figure 18: Observation 11, 8ks bins.

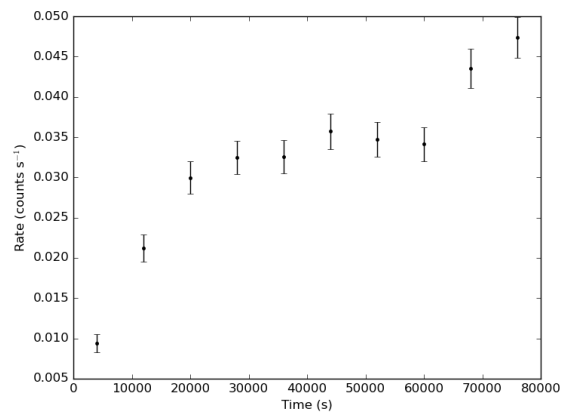


Figure 19: Observation 12, 8ks bins.

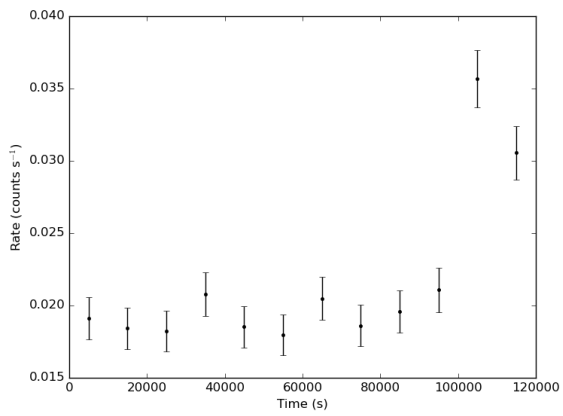


Figure 20: Observation 13, 10ks bins.

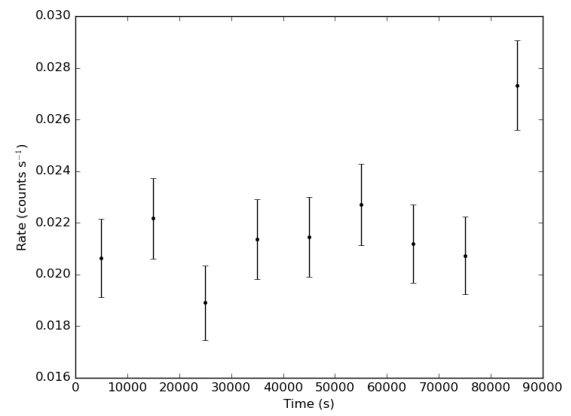


Figure 21: Observation 14, 10ks bins.